remote sensing

MDPI

Article

# Improved Geoarchaeological Mapping with Electromagnetic Induction Instruments from Dedicated Processing and Inversion

**Anders Vest Christiansen [1,*], Jesper Bjergsted Pedersen [1], Esben Auken [1], Niels Emil Søe [1], Mads Kähler Holst [2] and Søren Munch Kristiansen [1]**

[1] Department of Geoscience, Aarhus University, Høegh-Guldbergs Gade 2, 8000 Aarhus C, Denmark; jesper.bjergsted@geo.au.dk (J.B.P.); esben.auken@geo.au.dk (E.A.); nes@geo.au.dk (N.E.S.); smk@geo.au.dk (S.M.K.)

[2] Section for Archaeology, Department of Culture and Society, Aarhus University/Moesgaard Museum, Moesgård Alle 15, DK-8270 Højbjerg, Denmark; mads.holst@cas.au.dk

* Correspondence: anders.vest@geo.au.dk; Tel.: +45-2945-4305

Academic Editors: Kenneth L. Kvamme, Richard Müller and Prasad S. Thenkabail
Received: 6 September 2016; Accepted: 6 December 2016; Published: 14 December 2016

**Abstract:** Increasingly, electromagnetic induction methods (EMI) are being used within the area of archaeological prospecting for mapping soil structures or for studying paleo-landscapes. Recent hardware developments have made fast data acquisition, combined with precise positioning, possible, thus providing interesting possibilities for archaeological prospecting. However, it is commonly assumed that the instrument operates in what is referred to as Low Induction Number, or LIN. Here, we detail the problems of the approximations while discussing a best practice for EMI measurements, data processing, and inversion for understanding a paleo-landscape at an Iron Age human bone depositional site (Alken Enge) in Denmark. On synthetic as well as field data we show that soil mapping based on EMI instruments can be improved by applying data processing methodologies from adjacent scientific fields. Data from a 10 hectare study site was collected with a line spacing of 1–4 m, resulting in roughly 13,000 processed soundings, which were inverted with a full non-linear algorithm. The models had higher dynamic range in the retrieved resistivity values, as well as sharper contrasts between structural elements than we could obtain by looking at data alone. We show that the pre-excavation EMI mapping facilitated an archaeological prospecting where traditional trenching could be replaced by a few test pits at selected sites, hereby increasing the chance of finding human bones. In a general context we show that (1) dedicated processing of EMI data is necessary to remove coupling from anthropogenic structures (fences, phone cables, paved roads, etc.), and (2) that carrying out a dedicated full non-linear inversion with spatial coherency constraints improves the accuracy of resistivities and structures over using the data as they are or using the Low Induction Number (LIN) approximation.

**Keywords:** geophysical prospecting; near-surface geophysics; electromagnetic induction; archaeological prospecting; processing; inversion

## 1. Introduction

Increasingly, geophysical methods are used in archaeological prospecting, i.e., to help to distinguish between archaeological constructions and non-anthropogenically disturbed soils, or to make large-scale investigations to study paleo-landscapes. A review of geophysical methods in archaeology by Gaffney [1] summarized the most commonly used methods. Ground-penetrating radar (GPR) has been applied in many contexts, and with a varying degree of success, although buried stone structures are especially easily detected [2]. Various forms of magnetic prospecting were, and are,

the most frequently used geophysical technique for locating and delimiting archaeological resources [3]. Gaffney [1] stated that electromagnetic induction (EMI) techniques remained underestimated, as the Geonics EM38 system was the only one used at this time. Recently, several instruments and mountings have been tested with more advanced multi-receiver EMI instruments on archaeological sites. This includes Bonsall et al. [4] with an instrument from GF instruments (CMD mini-explorer), Bates [5] used EM31 and EM34 to map a paleo-landscape, while De Smedt et al. [6] and De Smedt et al. [7] have used DualEM-21s to map soil, buried objects, and archaeological features. These studies open for fast data acquisition combined with precise positioning by GPS, providing interesting possibilities for archaeological prospecting. The use of EMI methods has also been increased use outside the archeological community, especially for geotechnical applications and agricultural uses [8–14].

It is a common assumption for most of the above-mentioned applications that the instrument operates in what is referred to as low induction number, or LIN. Basically, this means that changing the frequency has no effect on the signal, or vice versa, that the investigation depth is independent of the subsurface resistivity for a fixed frequency [15]. The LIN approximation has the advantage that a very simple and linear relationship can be established between the signal and the subsurface resistivity structure [16–19]. The errors introduced by the LIN approximation are discussed in detail in Materials and Methods. The LIN approximation has been used by several authors, such as Santos [20], who created a laterally-constrained inversion routine, and it has also seen use in archaeological applications [21,22]. The approach by Santos was lately developed further to a quasi-3D approach, but still under the LIN approximation [23]. Other studies have also aimed at deriving the layering of the subsurface while assuming the LIN-approximation [24–26]. However, even if the LIN approximation is easy to use and implement, there has been a consistent use of the direct measurement values (typically converted to apparent conductivity or resistivity) as the final product [11,27,28]. Given that any electromagnetic (EM) method in the low frequency range [16] is diffusive and integrates a large volume based on the footprint of the system, this approach will inevitably smoothen out real soil structures. A few authors have suggested to perform a full inversion of the EMI data without assuming the LIN approximation [29–31], but it is our impression that this is not common practice. For airborne instruments of a similar type, the industry standard has been to perform a full processing and inversion of the data [32,33].

As a key aspect of this paper, we wish to advocate using a full solution to build a model instead of models based on approximations in future geoarchaeological and paleo-landscape EMI studies. The reasons are:

- The EM fields from an EMI instrument are diffusive and will average over a certain volume depending on the instrument design. Hence, a given data point never reflects a certain place in space. The deeper the target depth, the larger the averaging volume.
- Calculating the full forward response is computationally efficient, making CPU time negligible.
- Dedicated tools for continuous datasets, such as Aarhus Workbench [34], are ready off-the-shelf.
- The full solution provides a more robust interpretation of the archaeological and geological features than derived via approximations or raw data analysis.

We hypothesize in the present study that soil mapping by geophysical prospection can be improved by applying best-practice data processing methodologies from adjacent scientific fields. Our specific aims are (1) to show that dedicated processing of the data is necessary to assign relevant noise levels and to remove unwanted coupling from human-made structures (fences, phone cables, road barriers, etc.), and (2) to show that carrying out a dedicated full non-linear inversion with spatial coherency constraints improves the accuracy of resistivities and delineation of structures over interpretations directly from the raw instrument data or from using the LIN approximation. The software used has been developed for airborne EM data, but can be readily used for EMI data, as well [35]. We will explore these hypotheses and show how dedicated treatment of the EMI data improved soil mapping at a site where an ancient landscape was of archeological interest.

## 2. Materials and Methods

### *2.1. Study Site*

The study site is Alken Enge in Denmark (see Figure 1) where previous excavations have revealed a deposition of human bones of a presumed defeated army around 0–50 AD. The site is a part of the Illerup Ådal system where various forms of ritual depositions dating to the 3rd century BC to 5th century AD have been found in lake deposits. Alken Enge is a present-day fenland (circa 70 hectare) situated behind the eastern shores of the large Lake Mossø. The site has been known since the 19th century when peat digging uncovered human remains. Since 2009 new archaeological excavations have been initiated. Already during the first years investigations it became clear that human bones from at least 3–400 individuals were distributed within and particularly along the shores of a paleo lake in the present-day Alken Enge fenland, and that a complete excavation would be very comprehensive. The site, where the main deposition of bones were recovered by peat digging is today covered by a mosaic of private houses, gardens, wet meadows, and dense woodland, which renders large parts of the site inaccessible to excavation and intensive archaeological prospections by ditches and test pits proved difficult and expensive. Prior to further archaeological excavations and auguring, non-destructive EMI mapping was chosen as a cost-efficient alternative to delineate the paleo lake shores and associated channels.

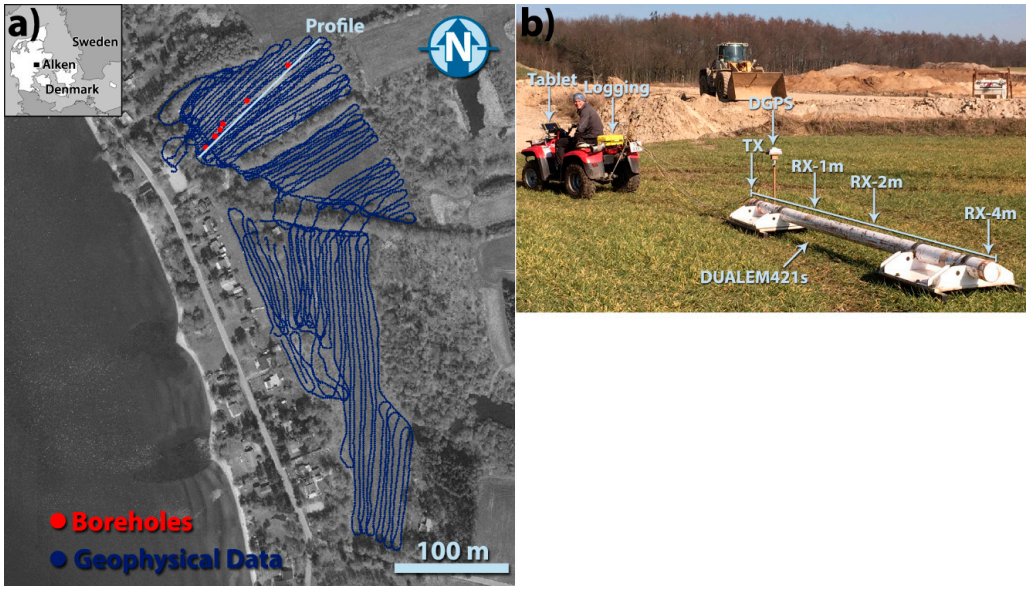


**Figure 1.** (**a**) Location of survey area and collected borehole and geophysical data. The map spans (552,960 m–553,420 m) in UTMX and (6,211,130 m–6,211,677 m) in UTMY (wgs84, zone 32°N). All following maps are exactly the same (**b**) Schematics of the DualEM-421s system employed in the survey (photo from another site).

### *2.2. Instrumental Setup and Field Work*

The DUALEM-421s sensor (from DualEM, Milton, Ontario, Canada) dual-geometry receivers, placed at distances of 1-, 2-, and 4-m from the transmitter, provide simultaneous readings of the quadrature (Q) and in-phase part (I) of the received secondary signal, most often stated as ppm or ppt with respect to the primary signal. The Q-part is often transformed to an apparent resistivity, $\rho_a$, using [16]:

$$\rho_a = \frac{\omega \mu_0 s^2}{4} \frac{Q_{primary}}{Q}, \quad (1)$$

where $s$ is the coil spacing, $\omega = 2\pi f$ is the angular frequency for the frequency, $f$, and $\mu_0 = 4\pi 10^{-7}$ is the magnetic permeability of free space. This allows for easy transformation of the data into a meaningful parameter.

At each distance the receivers are arranged horizontally (HCP configuration) and vertically (PRP configuration). The different coil configurations senses different volumes of the ground, which allows for analysis of the resistivity distribution in the top 6–8 m of earth.

The instrument was mounted on two non-metallic sledges, 4 m behind an all-terrain vehicle (ATV), and the front sledge was equipped with a rotational element for easy operation (Figure 1b). A real-time differential GPS (DGPS) is located above the transmitter (see Figure 1b) and all communication and data handling is controlled from an in-house developed logging system, which is controlled from a PC at the ATV. The driver has access to a tablet PC with a GIS map on which intended survey lines are drawn and actual positions are continuously shown for accurate navigation. Positioning and instrument readings can likewise be viewed in real-time on the tablet in order to evaluate if some areas have to be mapped more densely.

The geophysical field campaign was carried out in May 2014, during a period of dry weather. A 10 hectare study site was mapped in 2.5 h with a detailed line spacing of approximately 3 m (varying between 1 and 4 m defined by accessibility) (Figure 1a). The data were sampled at a rate of 10 Hz at a maximum speed of 15 km/h to maintain a lateral resolution capable of resolving structures of a few meters [36]. Prior to the EMI survey a soil auguring campaign was carried out on a larger area [37] in order to compare the geophysical results with ground truth. Inside the 10 ha survey area a total of six hand-auger drillings were performed to a depth of 1 to 12 m in a profile extending from the current lake shore and inlands (Figure 1), and the profile walls of several archaeological excavations were examined as well.

Prior to the field campaign the instrument was calibrated using an approach close to the one suggested by Lavoue [38]. Though, a word of caution is required with respect to calibration using models acquired from ERT measurements, which have inherent equivalences. The equivalence issues impose a risk that a range of different models fit the ERT data equally well, while in the EM data the difference in the responses produced by these models might be far larger than the anticipated calibration. At the field site the data levels were validated at a test-site before and after data collection to ensure consistent results.

### *2.3. Data Processing and Modelling*

The processing of the DualEM-421s data was carried out in the Aarhus Workbench [34], which is a dedicated program package for management, processing, inversion, and visualization of geophysical data and models in a fully-featured GIS environment. Key elements of the program are designed for airborne EM processing [35] and these features can be transferred directly to the processing and inversion of EMI data, which are essentially the same, i.e., continuous and electromagnetic.

Upon import the individual channels are shifted according to their individual lateral center point with respect to the position of the GPS. The lateral center points are defined as the mid-points between the individual transmitter and receiver pairs. The processing then consists of the following elements, which are summarized in Figure 2:

- Negative data are removed.
- Manual inspection of the raw data series with the primary target to identify couplings to human-made structures as buried cables, pipelines, metal fences, etc. Coupling effects are often easily identified by inspecting the GIS map with wire-installations shown together with the raw data. Figure 2a shows the full dataset with red dots whereas the superimposed blue dots show the resulting dataset after manual removal of couplings and noisy data. Figure 2b shows an example of a coupling in the dataset, which arises from a powered pump station. The effect of the manual processing for the entire survey is shown in the results section.

- The data are then averaged to improve the S/N-ratio. This is done by a running mean with a specified filter length, followed by a polynomial fit. The running mean filter length is typically in the order of 2–10 m, depending on the signal to noise ratio and the geological variability at hand. As the filter is a function of distance and not time, the number of measurements included in the filter will vary with the acquisition speed. In this process, great care is needed to make sure that geological structures are not smeared out by the averaging. Figure 2b shows a stretch of survey line with raw data as well as averaged data. Here, the averaging filter was set at 5 m.
- The averaged data are assigned noise according to (1) the absolute signal level with respect to absolute noise thresholds for the individual channels, and (2) the variance of the data entering the median filter. Here, the absolute noise level was set uniformly on all six channels to 0.6 mS/m based on on-site repetitive measurements. A sound estimate of noise-levels on the data are crucial for making a meaningful inversion later.
- Soundings for inversion are taken out at user-specified intervals, typically every 1–5 m. The trade-off is between computation speed and redundant information. There is no risk in choosing too low a sounding distance, but the soundings will then contain a lot of redundant information and the computation time for the subsequent inversion will go up. Here, a sounding distance of 1 m was chosen as some of the paleo-structures were thought to be quite small. The total number of raw measurements were 90,949. After processing and with one sounding every 1 m the total number of datasets (each with six data points) ready for inversion ends at 13,043.

The full processing cycle took about two hours. The majority of the removed data was removed along the road, were one would expect a higher degree of electrical installations.

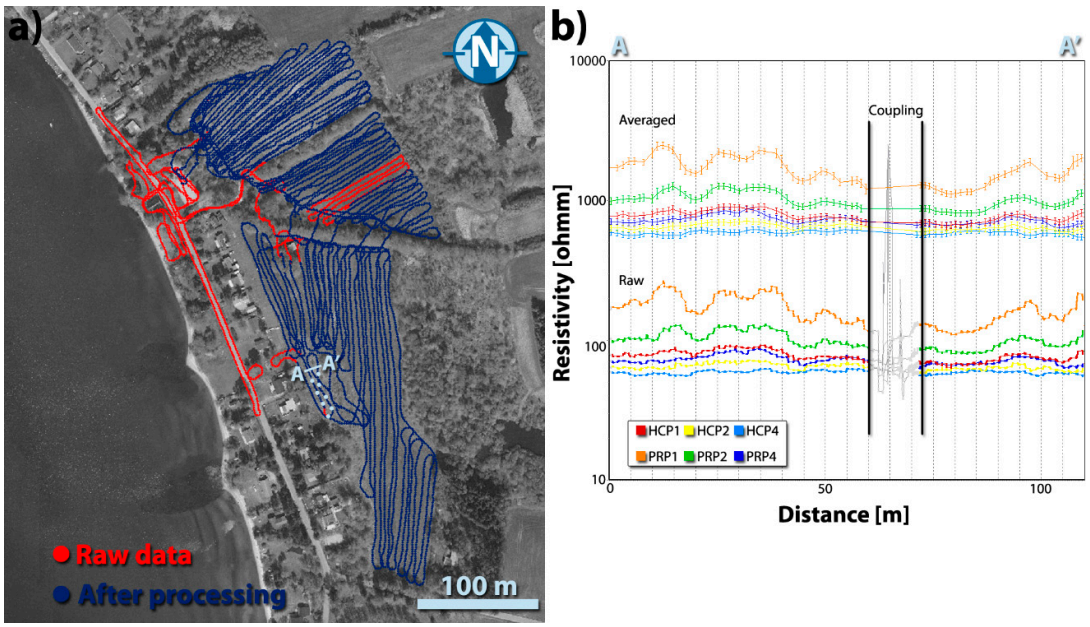


**Figure 2.** (**a**) The combined red and blue dots show the full datasets prior to processing, i.e., where it was physically possible to access the study site with the DualEM-421S system. The red dots show the datasets that were removed during the processing mainly due to coupling with man-made structures. The light blue dots between A and A′ indicates the track shown in (**b**). The map spans (552,960 m–553,420 m) in UTMX and (6,211,130 m–6,211,677 m) in UTMY (wgs84, zone 32°N). (**b**) Example of a coupling in the dataset and the effect of the averaging filters. The raw data show actual measured apparent resistivities whereas the averaged data have been shifted upwards by a factor of 10. The data affected by coupling to human-made structures are marked with grey.

After processing, the soundings were inverted. The backbone of the inversion routine is the fully non-linear AarhusInv code [39], which is used extensively for ground-based EM data, as well as airborne [40–42]. The forward response is 1D without approximations, such as the LIN approximation. The 1D forward response is very fast with the computation of roughly 1000 model responses per second on a single thread on a 'standard' office computer. Hence, we argue that computation speed cannot be used as an argument to adopt approximate solutions. Furthermore, a quasi-3D behavior in the model space is achieved through a spatially-constrained inversion algorithm [43], which adds constraints between model parameters both in-line and cross-line adding information on model consistency between proximal soundings. The connections of the spatial constraints are determined by a Delaunay triangulation creating a natural connection pattern between soundings based on the nearest neighbor principle, as shown in Figure 3. The strength of the spatial constraints are scaled linearly with distance, which effectively disables constraints between models that are far from each other.

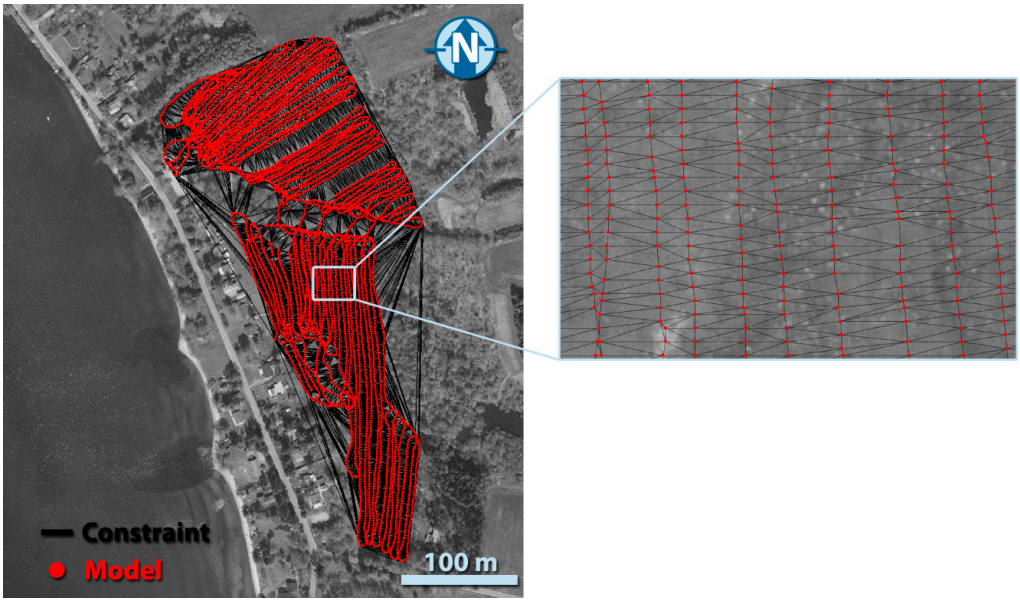


**Figure 3.** Map showing the spatially-constrained inversion concept with inline and cross-line constraints at Alken Enge. Sounding positions are marked with red dots and the interconnecting constraints are indicated with the black lines. The map spans (552,960 m–553,420 m) in UTMX and (6,211,130 m–6,211,677 m) in UTMY (wgs84, zone 32°N).

The output of the inversion is followed by a linearized estimate of the model covariance, i.e., the validity of the estimated model (not shown). This estimate only makes sense if the uncertainty numbers assigned to the data are meaningful as discussed earlier. The output is also supported by a noise-normalized data misfit number, which indicates to which degree the measured data can be reproduced by the proposed model. A misfit lower than one indicates that data are fitted within the estimated uncertainty (or error bar), and vice versa for misfits higher than one (Figure 4) and, obviously, the data misfit is a key quality control parameter when evaluating the output of the inversion routine and the validity of specific models. Without an estimate of the data fit it is essentially impossible to evaluate a suggested model, as it might not agree with the observed data. In the case below, we see that the data misfit increases where we have the higher resistivities, which is to be expected, as this is also where we have the lowest signal levels and, thereby, lower S/N ratios.

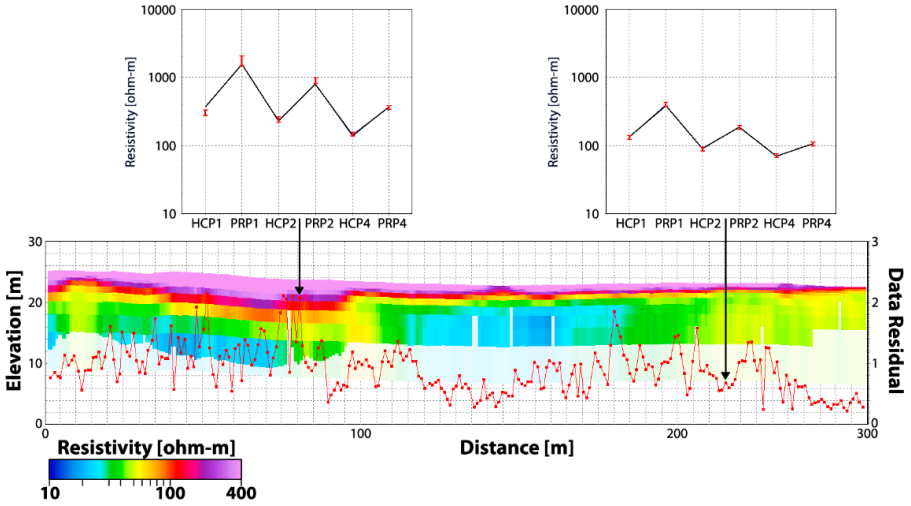


**Figure 4.** Panel showing an inverted resistivity section with data residuals as a tool for quality assessment of the inversion results. In the top panels the data are shown with red error bars and the forward response from the inverted model with the solid black line. Below the inverted model is shown with the data misfit in red. The arrows indicate the positions of the data plots on the full section.

### *2.4. Comparing Approximate Modelling and Full Non-Linear Solution*

The simplest approximation is to use the acquired data as they are and make interpretations directly on the structures as they are seen [11,27,28]. The lateral positioning of structures is fairly good with this approach, but inference of resistivity at a given depth will be highly uncertain as we will show here.

The most common approximation is the LIN-approximation as introduced above where a linear relationship between data and model space is established for easy transformation of data into models. The error introduced by the LIN approximation increases with a decreasing resistivity and by simple forward calculations comparing the full solution with the LIN solution for a 4 m coil separation with vertical dipoles at the surface of the earth operating at 9000 Hz (the longest configuration in the DualEM-421s instrument) we find that a 10% error on measured conductivities is reached at 15.9 mS/m or 64 ohm-m. At 3.9 mS/m, or 258 ohm-m, the error is at 5%.

To illustrate the difference further we will look at the synthetic model suites in Figure 5. The models all contain two layers and belong to either a conductive (10 ohm-m) over a resistive (100 ohm-m) type of model or the opposite (resistive over conductive). The figure illustrates the varying surveying depths encountered over varying geologies. We will use the term depth of investigation (DOI) when referring to the full solution which follows Christiansen and Auken [44], and the term depth of exploration (DOE) as suggested by DualEM [45] when referring to the LIN approximation. They are both measures of the maximum depth of investigation on a given model, and the DOI is considered the true value given that it is based on the full solution. The DOI computation uses all six data points of the DualEM-421s (Xs in Figure 5) and we compare this with an estimate of DOE from the longest (deepest) configuration, which is 1.5 times the spacing, or 5.8 m if carried 0.2 cm above the ground as in our case. It is seen from Figure 5 and the tabulated values in Table 1 that in the case of a conductive cover the measurements predicted by the LIN-approximation, stated as apparent resistivities, are not far from those actually achieved, but the surveying depth is vastly over-estimated with the LIN approximation comparing the DOI and DOE numbers. With the opposite model, the DOI and DOE estimates are closer, but the predicted LIN-measurements are quite far from the true ones. Note also that looking at the measured data over these models (predicted data from the full solution) it is quite difficult to infer anything about the true model structures. The reason is that the EM field is diffusive and states an

average value sampled over a volume rather than at a given depth. Lastly, it is worth noting that any errors listed here are increased if the carrying height of the instrument is not accounted for.

In other words, by looking only at data values, they will not represent a given depth and their values will reflect an average over a volume. Using the LIN-approximation DOI-numbers will introduce larger errors and the expected measurements cannot be predicted correctly. These conclusions are less prominent over highly resistive grounds where the LIN approximation is less inaccurate. In the results section we will show the difference between channel-values and inverted models as well the differences in DOI from real data.

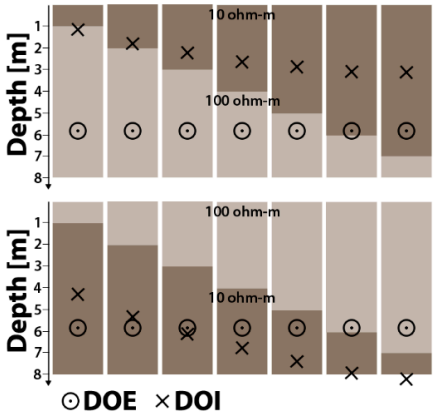


**Figure 5.** Survey depth of the DualEM-421s for two-layer models. The circles indicate *the depth of exploration (*DOE) stated by DualEM for the 4 m HCP configuration and assuming a low induction numbers (LIN) approximation. Crosses are DOI estimates obtained with a full solution of all six channels of a DualEM-421S instrument. Values are tabulated in Table 1.

**Table 1.** Comparison of LIN approximation with full solution. The table shows first the difference between the depth of investigation (DOI) computation from the full solution with the depth of exploration (DOE) computation from the LIN-approximation. Next, the table compares predicted measurements stated as apparent resistivities, $\rho_a$, (Equation (1)) from the full solution and the LIN-approximation.

| Thickness, Upper Layer | 1 m | 2 m | 3 m | 4 m | 5 m | 6 m | 7 m |
|---|---|---|---|---|---|---|---|
| **10/100 ohm-m Model** | | | | | | | |
| DOI, full, all (m) | 1.2 | 1.8 | 2.3 | 2.7 | 2.9 | 3.1 | 3.2 |
| DOE, 4 m HCP (m) | 5.8 | 5.8 | 5.8 | 5.8 | 5.8 | 5.8 | 5.8 |
| Abs error (m) | 4.6 | 4.0 | 3.5 | 3.1 | 2.9 | 2.7 | 2.6 |
| $\rho_a$ (4 m HCP, LIN) (ohm-m) | 44.7 | 25.6 | 19.3 | 16.4 | 14.9 | 13.9 | 13.3 |
| $\rho_a$ (4 m HCP, true) (ohm-m) | 47.2 | 26.7 | 20.1 | 17.2 | 15.7 | 14.8 | 14.3 |
| **100/10 ohm-m Model** | | | | | | | |
| DOI, full, all (m) | 4.3 | 5.3 | 6.1 | 6.8 | 7.4 | 7.9 | 8.3 |
| DOE, 4 m HCP (m) | 5.8 | 5.8 | 5.8 | 5.8 | 5.8 | 5.8 | 5.8 |
| Abs error (m) | 1.5 | 0.5 | −0.3 | −1.0 | −1.6 | −2.1 | −2.5 |
| $\rho_a$ (4 m HCP, LIN) (ohm-m) | 11.4 | 14.1 | 17.2 | 20.3 | 23.4 | 26.3 | 29.0 |
| $\rho_a$ (4 m HCP, true) (ohm-m) | 15.6 | 20.4 | 26.6 | 33.5 | 40.8 | 48.0 | 55.1 |

## 3. Results and Discussion

### *3.1. Geophysical Results and Borehole Comparison*

The results of the EMI survey are presented in Figure 6 as a cross-section and two interval resistivity maps. They reveal several small-scale resistivity structures, which can be related to soil/geological units of archeological importance. The cross-section highlights the correspondence

between geology and geophysics (Figure 6a), and the geophysical results are plotted as model bars with superimposed boreholes. In the first 20 m of the section high resistivities are found in the top part and the boreholes suggest this to be sand. The rest of the section has resistivities in the range of 40–100 ohm-m in the first meter identified as dry peat sediments. The lake sediments, the organic rich silts (gyttja), are seen as a low-resistivity layer below the peat or sand with a resistivity of 10–40 ohm-m. There is no distinct resistivity contrast identified between the lake sediments with or without carbonates.

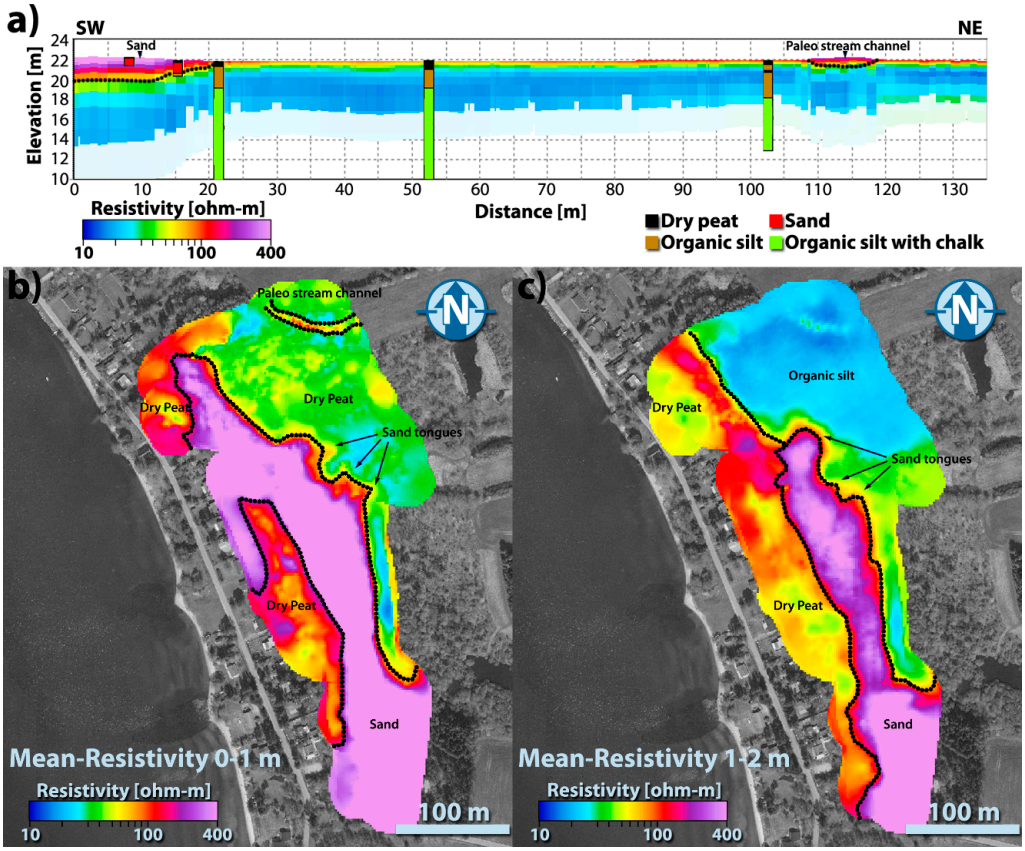


**Figure 6.** (**a**) Geophysical section with borehole information at Alken Enge. The model is from a full non-linear inversion of the entire data set. The location of the profile can be seen in Figure 1a; (**b**) Mean-resistivity map in a depth of 0–1 m; (**c**) Mean-resistivity map in a depth of 1–2 m. The map spans (552,960 m–553,420 m) in UTMX and (6,211,130 m–6,211,677 m) in UTMY (wgs84, zone 32°N).

The sand layer (coordinate 0–20 m; Figure 6a–c) is a well-resolved unit with a thickness of about 2 m, and the lower boundary is clearly identified due to the good resistivity contrast between the sand and underlying organic-rich silt. The thin top-layer of dry peat is also clearly identified in the geophysics above the organic-rich silt sediments. The peat sediments stand out as a fairly resistive layer since the resistivity of peat is highly dependent on the water content, and the mapping was carried out in a dry period. Boreholes in a profile distance 22, 52, and 102 m, confirming a good shallow resolution, verify the thickness of the thin dry peat layer from the geophysics. In a profile distance of 110–118 m a 1–2 m thick sand layer is seen in the middle of the wetland. Historical maps of land-use in the area document that a stream channel used to run perpendicular to the drawn profile at this profile distance. The actual path of a paleo-stream channel (>150 years old but younger than the human bone deposition event) can be tracked by visualizing the geophysical results as interval resistivity maps (Figure 6b,c) as the channel contains more sand than the surrounding sediment. The interval resistivity maps show the resistivity in depths of 0–1 m and 1–2 m, and have been created by means of ordinary

kriging interpolation with a search distance of 20 m, where the semi-variograms have been fitted for the intervals individually. The sandy paleo-stream channel stands out as a resistive anomaly in the Alken Enge wetland in 0–1 m depth, with a width varying from 5–10 m.

The spatial distribution of the sandy sediments is also identified by the interval resistivity maps with several "sand tongues" extending into the organic-rich silty sediments (Figure 6b,c), likely caused by the proximal spits from a continuous S to N spit-formation [37]. The evolution of these sand tongues can be investigated by inspection of the interval resistivity maps in different depth intervals. The sand tongues are also of archeological importance, since it can be hypothesized that human depositions in open water or at the coast would be concentrated at the shores of the spit extending into the paleo-lake.

### *3.2. Comparing Data Values with Full Solution on the Field Case*

The following will illustrate the difference between using the data as they were collected and making an actual full, non-approximate inversion. Figure 7 compares the measured channel values (2 m HCP) with an interval resistivity map. Under the LIN-approximation the 2 m HCP channel has a focus depth, half of the DOE, of 1.5 m. These channel values are displayed in Figure 7a. Assuming that these data represent the resistivities at that depth we will now compare with a full inversion extracting resistivity values at the same depth. In Figure 7b we show the actual resistivities obtained for that depth by slicing through the inverted models. As expected the overall resistivity structures are similar between the two images, but the boundaries are clearer and the true dynamic range of resistivities (Figure 7b) are larger than what is recovered from the channel values. This is especially evident for the sand tongues and the paleo-stream channel.

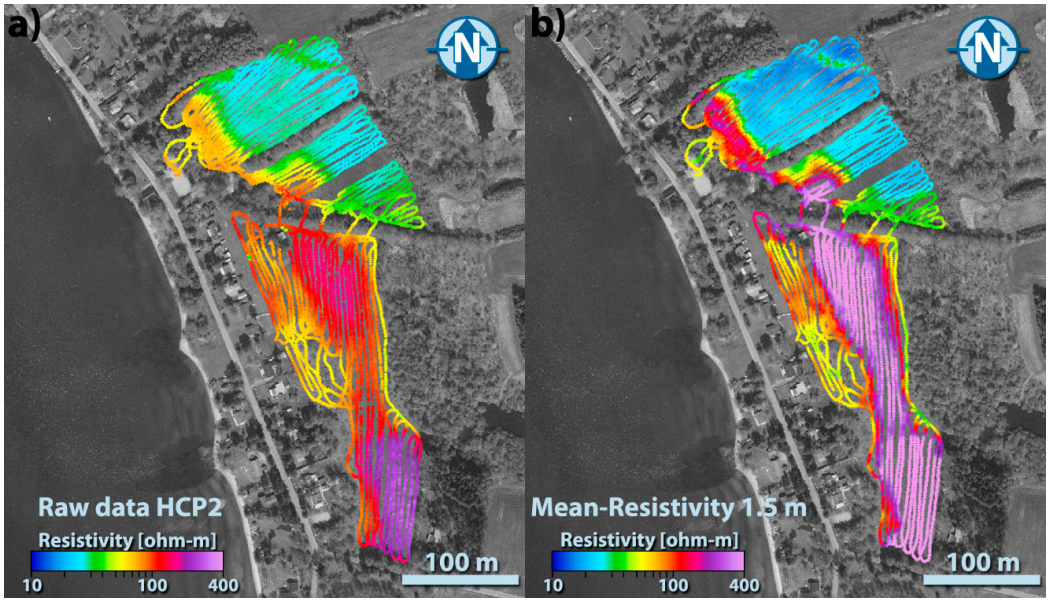


**Figure 7.** Comparison between the channel values of the HCP2-channel which is reported to have a focus depth of 1.5 m, and the full solution for the Alken Enge field case. (**a**) Raw channel data values for the 2 m horizontal co-planar receiver; (**b**) Mean-resistivity map in a depth of 1.5 m based on the full solution. The map spans (552,960 m–553,420 m) in UTMX and (6,211,130 m–6,211,677 m) in UTMY (wgs84, zone 32°N).

Another advantage of the full solution is that a depth of investigation (DOI) is calculated for each resistivity model [44]. The DOI as displayed in Figure 8 utilizes the actual recovered resistivity model for each of the sounding positions in the Alken Enge case. In the paleo-lake east of the sandy spit, where the thickness of the low-resistivity organic-rich silty lake sediment is great, the depth of investigation is only 3 m in some places. On the other hand, in areas where a thick sand sequence

overlies the low-resistivity organic silt, the DOI is 7–9 m. For the Alken Enge field case the overall data quality was good and, hence, the resistivity model is the driving factor for the DOI. If the data quality is poor, the DOI will mimic this by being shallower. Hence, proper understanding of the DOI is crucial for a trustworthy paleo-landscape interpretation of the geophysical results, which is evident by comparing the DOI value range for the Alken Enge case study with the assumed uniform DOE of about 6 m from the LIN approximation, as reported from Table 1.

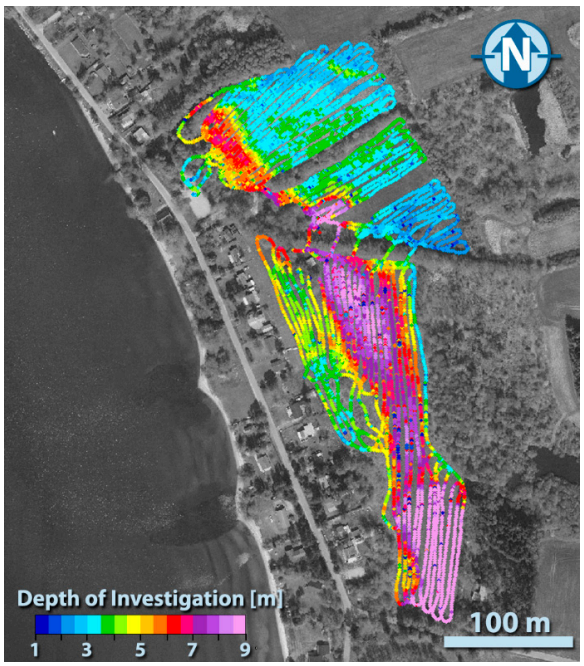


**Figure 8.** Depth of investigation, DOI, for the individual resistivity models at Alken Enge. The map spans (552,960 m–553,420 m) in UTMX and (6,211,130 m–6,211,677 m) in UTMY (wgs84, zone 32°N).

The results of the pre-excavation EMI mapping campaign were used to compile a detailed 3D image of the paleo landscape at Alken Enge. In turn, this facilitated an archaeological prospecting where traditional trenching in approximately 10% of the area could be replaced by few test pits at sites selected in relation to the paleo-lake's shores. The chance of finding human bones could, thus, be evaluated in a consistent manner and improve the understanding of the post-battle sacrificial practice. In respect to an improved paleo-landscape understanding, the 3D EMI survey delineated the spit structures in detail, and was very useful for focusing and minimizing the number of boreholes and excavation pits. Next, even the shape of the sandy spit deposit could be evaluated having a convex bottom-boundary from the resistivity depth-profile (Figure 6a), likely an effect of increasing subsidence below the central part of the N–S elongated coastal spit as most material here is deposited on top of the non-consolidated organic-rich lake deposit underlying the entire spit [46].

Intensive geoarchaeological and geomorphological investigations at the site after the EMI mapping has revealed that the deposited human bones were situated on the shores of a spit/barrier-coast system and in one paleo-channel between two lakes. Studies that combine various data types and interpret the geomorphology, geoarchaeological, and in situ preservation conditions at Alken Enge have been reported recently [37,46,47].

### *3.3. Evaluating the Benefit of Processing the Data before Inversion*

Finally, to visualize the effect of dedicated processing as described in Section 2, Figure 9 shows identical plots to those displayed in Figure 7, but where no processing has been done to the data. Boxes 1–4 indicate areas with examples of coupling effects that are dealt with in the manual processing.

Some effects appears in the raw data of some channels, but not others, while other effects are most clearly identified in the inverted models. Box 1 shows a coupling effect associated to a small shed. The effect is clearly visible in the raw data (Figure 9a), but is not seen in the mean resistivity map of the displayed depth (Figure 9b). Box 2 shows a part of the data where the tow cable had erroneously been too short because it had caught the wheel of the ATV, which introduced a coupling from the metal of the ATV into the receiver coils of the instrument due to the decreased distance. This effect is hardly visible on the channel displayed (Figure 9a), but clearly visible in inverted section as an offset in the resistivities (Figure 9b). Box 3 shows part of the couplings associated with installations in the road and connections to the houses. The effect is seen as both high and low anomalies in the raw data (Figure 9a), but mostly as a high-resistivity anomaly in the inverted models at the given depth (Figure 9b).

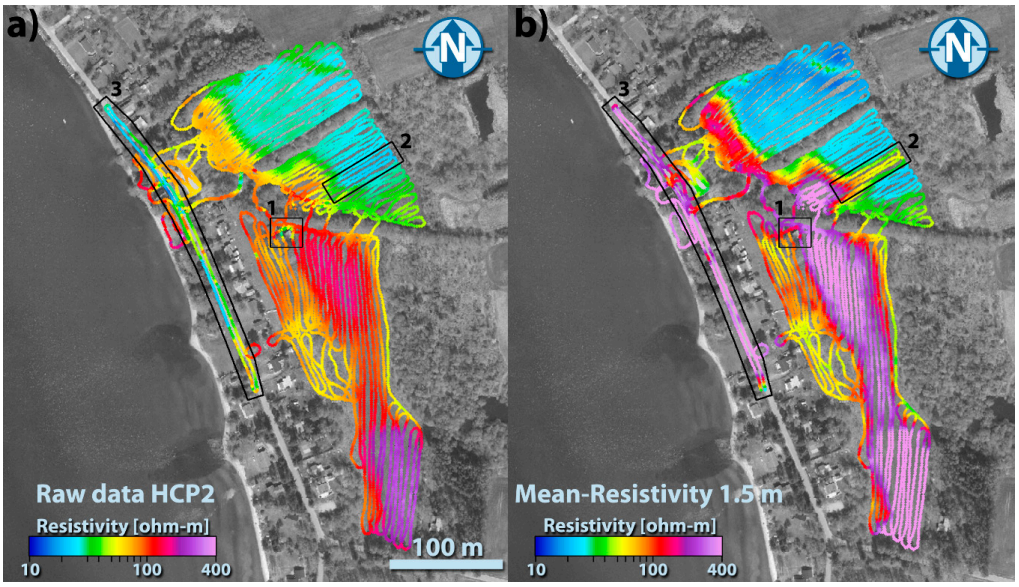


**Figure 9.** The effect of not doing any processing on raw data and in the resulting models. The display is identical to that of Figure 7, but here without processing. (**a**) Raw channel data values for the 2 m horizontal co-planar receiver; (**b**) Mean-resistivity map in a depth of 1.5 m based on the full solution. Boxes 1–4 indicate areas with examples of coupling effects that are dealt with in the manual processing. The map spans (552,960 m–553,420 m) in UTMX and (6,211,130 m–6,211,677 m) in UTMY (wgs84, zone 32°N).

Comparing Figure 9 with Figure 7 it is clear that many of the effects identified as couplings might have been easily interpreted as geological structures if they had not been removed in the manual processing step.

## 4. Conclusions

With the increasing use of EMI methods in paleo landscape investigations and archaeological prospection a need to establish best practice for data processing and inversion is needed. Traditionally, it is assumed that the EMI instruments operate in what is referred to as Low Induction Number (LIN), which supplies a simple linear relationship between the data and the models. We showed with synthetic data as well as field data that soil mapping based on EMI instruments is improved by applying best-practice data processing methodologies from the well-established approach in airborne electromagnetics. From synthetic models we show that with the LIN approximation the measurements cannot be predicted correctly and depth of investigation estimates might be vastly overestimated. This will inherently jeopardize interpretations based on the LIN-approximation.

In the Alken Enge case study, data from a 10 hectare site were collected with a line spacing of 1–4 m, resulting in roughly 13,000 processed soundings which were inverted with a full non-linear algorithm. The retrieved models had a higher dynamic range in the retrieved model values as well as sharper contrasts between larger structural elements than we could get by looking at data alone. Case-specifically we show that the pre-excavation EMI mapping facilitated an archaeological prospecting where traditional trenching could be replaced by fewer test pits at selected sites where, based on prior archaeological excavations, the EMI mapping, and 3D paleo landscape model, the chance of finding human bones was considered highest.

In general terms we have showed that (1) dedicated processing of the data is necessary to remove couplings from anthropogenic structures (fences, phone cables, road barriers, etc.), and (2) that carrying out a dedicated full non-linear inversion with spatial coherency constraints especially improves the vertical accuracy of the resistivity models over interpretations directly from the raw instrument data.

**Acknowledgments:** This work was supported by grants from the Carlsberg Foundation (No. 2012_01_0495), the Danish Agency for Culture and Aarhus University.

**Author Contributions:** For this research article the authors have contributed in the following way: Christiansen, A.V. proposed the idea of a detailed processing of the EMI data for enhanced model resolution and he wrote large sections of the paper. Pedersen, J.B. carried out the field work, processed the geophysical data, and wrote large sections of the paper. Auken, E. was the driving force in the design of the algorithms used for the processing and inversion used previously for airborne methods, and he played a key role in adapting them for the EMI instruments. Søe, N.E. carried out all the geological ground truthing and laid out the overall interpretation of the results in the geological context. Holst, M.K. was the driving force in setting up the entire project, contributed to the study's design and provided essential information in the interpretation of the results in the archaeological context at Alken. Kristiansen, S.M. contributed significant knowledge in the study's design, the interpretation of the results for soil properties and landscape evolution in general, and he contributed greatly to the writing of the paper.

**Conflicts of Interest:** The authors declare no conflict of interest.

## References

1. Gaffney, C. Detecting trends in the prediction of the buried past: A review of geophysical techniques in archaeology. *Archaeometry* **2008**, *50*, 313–336. [CrossRef]
2. Saey, T.; Van Meirvenne, M.; De Smedt, P.; Stichelbaut, B.; Delefortrie, S.; Baldwin, E.; Gaffney, V. Combining EMI and GPR for non-invasive soil sensing at the Stonehenge World Heritage Site: The reconstruction of a WW1 practice trench. *Eur. J. Soil Sci.* **2015**, *66*, 166–178. [CrossRef]
3. Linford, N.; Linford, P.; Martin, L.; Payne, A. Recent results from the English Heritage caesium magnetometer system in comparison with recent fluxgate gradiometers. *Archaeol. Prospect.* **2007**, *14*, 151–166. [CrossRef]
4. Bonsall, J.; Fry, R.; Gaffney, C.; Armit, I.; Beck, A.; Gaffney, V. Assessment of the CMD mini-explorer, a new low-frequency multi-coil electromagnetic device, for archaeological investigations. *Archaeol. Prospect.* **2013**, *20*, 219–231. [CrossRef]
5. Bates, M.R.; Bates, C.R.; Whittaker, J.E. Mixed method approaches to the investigation and mapping of buried Quaternary deposits: Examples from southern England. *Archaeol. Prospect.* **2007**, *14*, 104–129. [CrossRef]
6. De Smedt, P.; Saey, T.; Lehouck, A.; Stichelbaut, B.; Meerschman, E.; Islam, M.M.; De Vijver, E.V.; Van Meirvenne, M. Exploring the potential of multi-receiver EMI survey for geoarchaeological prospection: A 90ha dataset. *Geoderma* **2013**, *199*, 30–36. [CrossRef]
7. De Smedt, P.; Van Meirvenne, M.; Saey, T.; Baldwin, E.; Gaffney, C.; Gaffney, V. Unveiling the prehistoric landscape at Stonehenge through multi-receiver EMI. *J. Archaeol. Sci.* **2014**, *50*, 16–23. [CrossRef]
8. Jiang, P.P.; He, Z.Q.; Kitchen, N.R.; Sudduth, K.A. Bayesian analysis of within-field variability of corn yield using a spatial hierarchical model. *Precis. Agric.* **2009**, *10*, 111–127. [CrossRef]
9. Lopez-Lozano, R.; Casterad, M.A.; Herrero, J. Site-specific management units in a commercial maize plot delineated using very high resolution remote sensing and soil properties mapping. *Comput. Electron. Agric.* **2010**, *73*, 219–229. [CrossRef]
10. Eigenberg, R.A.; Woodbury, B.L.; Nienaber, J.A.; Spiehs, M.J.; Parker, D.B.; Varel, V.H. Soil conductivity and multiple linear regression for precision monitoring of beef feedlot manure and runoff. *J. Environ. Eng. Geophys.* **2010**, *15*, 175–184. [CrossRef]

11. Serrano, J.M.; Shahidian, S.; da Silva, J.R.M. Apparent electrical conductivity in dry versus wet soil conditions in a shallow soil. *Precis. Agric.* **2013**, *14*, 99–114. [CrossRef]
12. Everett, M.E. Theoretical developments in electromagnetic induction geophysics with selected applications in the near surface. *Surv. Geophys.* **2012**, *33*, 29–63. [CrossRef]
13. Doolittle, J.A.; Brevik, E.C. The use of electromagnetic induction techniques in soils studies. *Geoderma* **2014**, *223*, 33–45. [CrossRef]
14. Calamita, G.; Perrone, A.; Brocca, L.; Onorati, B.; Manfreda, S. Field test of a multi-frequency electromagnetic induction sensor for soil moisture monitoring in southern Italy test sites. *J Hydrol.* **2015**, *529*, 316–329. [CrossRef]
15. McNeill, J.D. *Why Doesn't Geonics Limited Build a Multi-Frequency EM31 or EM38?* Technical note TN-30; Geonics Limited: Mississauaga, ON, Canada, 1996.
16. McNeill, J. *Electromagnetic Terrain Conductivity Measurement at Low Induction Numbers*; Technical Report TN-6; Geonics Limited: Mississauga, ON, Canada, 1980.
17. Callegary, J.B.; Ferre, T.P.A.; Groom, R.W. Vertical spatial sensitivity and exploration depth of low-induction-number electromagnetic-induction instruments. *Vadose Zone J.* **2007**, *6*, 158–167. [CrossRef]
18. Callegary, J.B.; Ferré, T.P.A.; Groom, R.W. Three-dimensional sensitivity distribution and sample volume of low-induction-number electromagnetic-induction instruments. *Soil Sci. Soc. Am. J.* **2012**, *76*, 85–91. [CrossRef]
19. Wait, J.R. A note on the electromagnetic response of a stratified earth. *Geophysics* **1962**, *27*, 382–385. [CrossRef]
20. Santos, F.A.M. 1-D laterally constrained inversion of EM34 profiling data. *J. Appl. Geophys.* **2004**, *56*, 123–134. [CrossRef]
21. De Smedt, P.; Van Meirvenne, M.; Herremans, D.; De Reu, J.; Saey, T.; Meerschman, E.; Crombé, P.; De Clercq, W. The 3-D reconstruction of medieval wetland reclamation through electromagnetic induction survey. *Sci. Rep.* **2013**, *3*. [CrossRef] [PubMed]
22. Saey, T.; De Smedt, P.; Meerschman, E.; Islam, M.M.; Meeuws, F.; Van De Vijver, E.; Lehouck, A.; Van Meirvenne, M. Electrical conductivity depth modelling with a multireceiver EMI sensor for prospecting archaeological features. *Archaeol. Prospect.* **2012**, *19*, 21–30. [CrossRef]
23. Zare, E.; Huang, J.; Santos, F.A.M.; Triantafilis, J. Mapping salinity in three dimensions using a DualEM-421 and electromagnetic inversion software. *Soil Sci. Soc. Am. J.* **2015**, *79*, 1729–1740. [CrossRef]
24. Mester, A.; Van Der Kruk, J.; Zimmermann, E.; Vereecken, H. Quantitative two-layer conductivity inversion of multi-configuration electromagnetic induction measurements. *Vadose Zone J.* **2011**, *10*, 1319–1330. [CrossRef]
25. Dafflon, B.; Hubbard, S.S.; Ulrich, C.; Peterson, J.E. Electrical conductivity imaging of active layer and permafrost in an Arctic ecosystem, through advanced inversion of electromagnetic induction data. *Vadose Zone J.* **2013**, *12*. [CrossRef]
26. Jadoon, K.Z.; Moghadas, D.; Jadoon, A.; Missimer, T.M.; Al-Mashharawi, S.K.; McCabe, M.F. Estimation of soil salinity in a drip irrigation system by using joint inversion of multicoil electromagnetic induction measurements. *Water Resour. Res.* **2015**, *51*, 3490–3504. [CrossRef]
27. Lee, B.D.; Jenkinson, B.J.; Doolittle, J.A.; Taylor, R.S.; Tuttle, J.W. Electrical conductivity of a failed septic system soil absorption field. *Vadose Zone J.* **2006**, *5*, 757–763. [CrossRef]
28. Saey, T.; De Smedt, P.; De Clercq, W.; Meerschman, E.; Monirul Islam, M.; Van Meirvenne, M. Identifying soil patterns at different spatial scales with a multi-receiver emi sensor. *Soil Sci. Soc. Am. J.* **2013**, *77*, 382–390. [CrossRef]
29. Benech, C.; Dabas, M.; Simon, F.-X.; Tabbagh, A.; Thiesson, J. Interpretation of shallow electromagnetic instruments resistivity and magnetic susceptibility measurements using rapid 1D/3D inversion. *Geophysics* **2016**, *81*, E103–E112. [CrossRef]
30. Dabas, M.; Anest, A.; Thiesson, J.; Tabbagh, A. Slingram EMI devices for characterizing resistive features using apparent conductivity measurements: Check of the DualEM-421S instrument and field tests. *Archaeol. Prospect.* **2016**, *23*, 165–180. [CrossRef]
31. Triantafilis, J.; Wong, V.; Santos, F.A.M.; Page, D.; Wege, R. Modeling the electrical conductivity of hydrogeological strata using joint-inversion of loop-loop electromagnetic data. *Geophysics* **2012**, *77*, WB99–WB107. [CrossRef]
32. Siemon, B.; Christiansen, A.V.; Auken, E. A review of helicopter-borne electromagnetic methods for groundwater exploration. *Near Surf. Geophys.* **2009**, *7*, 629–646. [CrossRef]

33. Sengpiel, K.P.; Siemon, B. Advanced inversion methods for airborne electromagnetic exploration. *Geophysics* **2000**, *65*, 1983–1992. [CrossRef]
34. Auken, E.; Viezzoli, A.; Christiansen, A.V. A single software for processing, inversion, and presentation of AEM data of different systems: The Aarhus Workbench. In Proceedings of the International Geophysical Conference and Exhibition, Adelaide, SA, Australia, 22–25 February 2009; pp. 1–5.
35. Auken, E.; Christiansen, A.V.; Westergaard, J.A.; Kirkegaard, C.; Foged, N.; Viezzoli, A. An integrated processing scheme for high-resolution airborne electromagnetic surveys, the SkyTEM system. *Explor. Geophys.* **2009**, *40*, 184–192. [CrossRef]
36. Pedersen, J.B.; Auken, E.; Vest, C.A.; Kristiansen, S.M. Mapping soil heterogeneity using spatially constrained inversion of electromagnetic induction data. In Proceedings of the First Conference on Proximal Sensing Supporting Precision Agriculture, Turin, Italy, 6 September 2015.
37. Søe, N.E.; Odgaard, B.; Hertz, E.; Holst, M.K.; Kristiansen, S.M. Geological setting of a sacred landscape: Iron age post battle depositions at Alken Enge, Denmark. *Geoarchaeology* **2016**, submitted.
38. Lavoué, F.; Van Der Kruk, J.; Rings, J.; André, F.; Moghadas, D.; Huisman, J.A.; Lambot, S.; Weihermüller, L.; Vanderborght, J.; Vereecken, H. Electromagnetic induction calibration using apparent electrical conductivity modelling based on electrical resistivity tomography. *Near Surf. Geophys.* **2010**, *8*, 553–561. [CrossRef]
39. Auken, E.; Christiansen, A.V.; Fiandaca, G.; Schamper, C.; Behroozmand, A.A.; Binley, A.; Nielsen, E.; Effersø, F.; Christensen, N.B.; Sørensen, K.I.; et al. An overview of a highly versatile forward and stable inverse algorithm for airborne, ground-based and borehole electromagnetic and electric data. *Explor. Geophys.* **2015**, *46*, 223–235. [CrossRef]
40. Podgorski, J.E.; Green, A.G.; Kalscheuer, T.; Kinzelbach, W.; Horstmeyer, H.; Maurer, H.; Rabenstein, L.; Doetsch, J.; Auken, E.; Ngwisanyi, T.; et al. Integrated interpretation of helicopter and ground-based geophysical data recorded within the Okavango Delta, Botswana. *J. Appl. Geophys.* **2015**, *114*, 52–67. [CrossRef]
41. Mikucki, J.A.; Auken, E.; Tulaczyk, S.; Virginia, R.A.; Schamper, C.; Sorensen, K.I.; Doran, P.T.; Dugan, H.; Foley, N. Deep groundwater and potential subsurface habitats beneath an Antarctic dry valley. *Nat. Commun.* **2015**, *6*. [CrossRef] [PubMed]
42. Auken, E.; Violette, S.; d'Ozouville, N.; Deffontaines, B.; Sørensen, K.I.; Viezzoli, A.; de Marsily, G. An integrated study of the hydrogeology of volcanic islands using helicopter borne transient electromagnetic: Application in the Galápagos Archipelago. *Comptes Rendus Geosci.* **2009**, *341*, 899–907. [CrossRef]
43. Viezzoli, A.; Christiansen, A.V.; Auken, E.; Sørensen, K.I. Quasi-3d modeling of airborne tem data by spatially constrained inversion. *Geophysics* **2008**, *73*, F105–F113. [CrossRef]
44. Christiansen, A.V.; Auken, E. A global measure for depth of investigation. *Geophysics* **2012**, *77*, WB171–WB177. [CrossRef]
45. Taylor, R. Apparent Conductivity as an Indicator of Thickness. Available online: http://www.dualem.com/acit.htm (accessed on 5 September 2016).
46. Søe, N.E.; Odgaard, B.; Nielsen, A.B.; Olsen, J.; Kristiansen, S.M. The making of a sacred landscape: Late Holocene palaeoecology of Ilsø and the Illerup/Alken Enge valley, Denmark. *Veg. Hist. Archaeobothany* **2016**, submitted.
47. Tjelldén, A.K.E.; Matthiesen, H.; Petersen, L.M.M.; Søe, N.E.; Kristiansen, S.M. In-situ preservation solutions for deposited Iron age human bones in Alken Enge, Denmark. *Conserv. Manag. Archaeol. Sites* **2016**, *18*, 126–138. [CrossRef]